# Prediction of super-heavy $N^*$ and $\Lambda^*$ resonances with hidden beauty

Jia-Jun Wu[1] and B. S. Zou[1,2]

[1] Institute of High Energy Physics, CAS, P.O.Box 918(4), Beijing 100049, China

[2] Theoretical Physics Center for Science Facilities, CAS, Beijing 100049, China

(Dated: November 26, 2010)



## Abstract

The meson-baryon coupled channel unitary approach with the local hidden gauge formalism is extended to the hidden beauty sector. A few narrow $N^*$ and $\Lambda^*$ around 11 GeV are predicted as dynamically generated states from the interactions of heavy beauty mesons and baryons. Production cross sections of these predicted resonances in $pp$ and $ep$ collisions are estimated as a guide for the possible experimental search at relevant facilities.

## I. INTRODUCTION

In the classical quark models, all established baryons are ascribed into simple 3-quark (qqq) configurations [1]. The excited baryon states are described as excitation of individual constituent quarks, similar to the cases for atomic and nuclear excitations. However, unlike atomic and nuclear excitations, the typical hadronic excitation energies are comparable with constituent quark masses. Hence to drag out a $q\bar{q}$ pair from gluon field could be a new excitation mechanism besides the conventional the classical orbital excitation of original constituent quarks. Some baryon resonances are proposed to meson-baryon dynamically generated states [2–8] or states with large $(qqqq\bar{q})$ components [9–11]. A difficulty to pin down the nature of these baryon resonances is that the predicted states from various models are around the same energy region and there are always some adjustable ingredients in each model to fit the experimental data. A typical example is $N^*(1535)$ which has large couplings to the strangeness. In the 3-quark (qqq) configurations, it is described as the orbital angular momentum $L = 1$ excitation of a quark. But phenomenological studies suggest that it may be a quasi-bound state of $K\Sigma$ system [12–14], or as a hidden strangeness 5-quark state [10, 15]. In order to clearly demonstrate the new excitation mechanism and the corresponding states, in Ref.[16], the meson-baryon coupled channel unitary approach with the local hidden gauge formalism was performed for the hidden charm sector and several narrow $N^*$ and $\Lambda^*$ resonances with hidden charm were predicted to exist. If found experimentally, these resonances would definitely not be described as three constituent quark states. Here, we extend the study to the hidden beauty sector. Some super-heavy $N^*$ and $\Lambda^*$ resonances with hidden beauty are predicted to exist, with mass around 11 GeV and width smaller than 10 MeV. If these resonances can be experimentally confirmed, they should be part of the heaviest super-heavy island of $N^*$ and $\Lambda^*$ state. As a guild to the future experimental search for these new predicted states, their production cross sections in $pp$ and $ep$ collisions are estimated.

In the next section, we present the formalism and ingredients for the study of interactions between heavy beauty meson and baryon, and give some detailed discussion on the intermediate meson-baryon loop G functions. In the section.III, our numerical results for the masses and widths of the predicted super-heavy $N^*$ and $\Lambda^*$ states are given, followed by a discussion. In the section.IV, the calculation about production of these predicted states from $pp$ and $ep$ collisions is presented. Finally, a short summary is given in the last section.

## II. FORMALISM FOR MESON-BARYON INTERACTION

We follow the recent work of Ref. [16] on the interactions between charmed mesons and baryons, and replace charm quark by beauty quark. The $PB \to PB$ and $VB \to VB$ interactions by exchanging a vector meson are considered, as shown by the Feynman diagrams in Fig. 1.

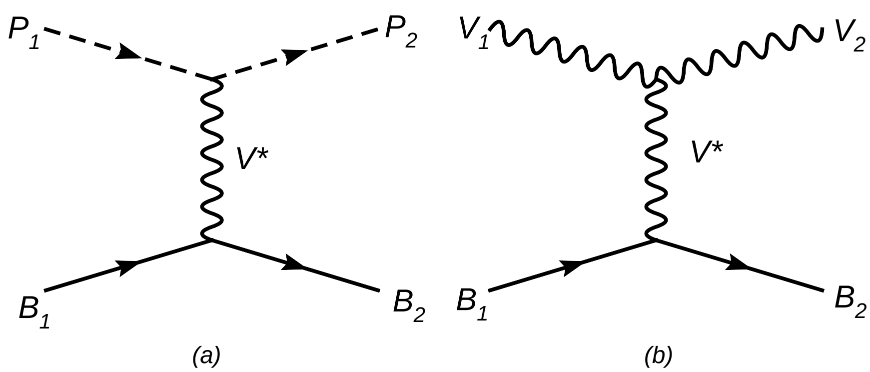


FIG. 1: Feynman diagrams for the pseudoscalar-baryon (a) or vector-baryon (b) interaction via the exchange of a vector meson ($P_1$, $P_2$ are $B^0$, $B^+$ or $B_s^0$, and $V_1$, $V_2$ are $B^{0*}$, $B^{+*}$ or $B_s^{0*}$, and $B_1$, $B_2$ are $\Sigma_b$, $\Lambda_b$, $\Xi_b$, $\Xi_b'$ or $\Omega_b$, and $V^*$ is $\rho$, $K^*$, $\phi$ or $\omega$).

The effective Lagrangians for the interactions involved are [17]:

$$\begin{aligned} \mathcal{L}_{VVV} &= ig\langle V^\mu [V^\nu, \partial_\mu V_\nu]\rangle \\ \mathcal{L}_{PPV} &= -ig\langle V^\mu [P, \partial_\mu P]\rangle \\ \mathcal{L}_{BBV} &= g(\langle \bar{B}\gamma_\mu [V^\mu, B]\rangle + \langle \bar{B}\gamma_\mu B\rangle\langle V^\mu\rangle) \end{aligned} \tag{1}$$

where $P$ and $V$ stand for pseudoscalar and vector mesons of the 16-plet of SU(4), respectively.

Using the same approach of Ref.[16], only the $\gamma^0$ component of Eq.(1) are taken, the three momentum versus the mass of the meson can be neglected under the low energy approximation. Similarly, the $q^2/M_V^2$ term in the vector meson propagator is neglected so that the propagator is approximately $g^{\mu\nu}/M_V^2$. Note when we consider transitions from heavy mesons to light ones later on, we perform the exact calculation without such approximation.

Then with $g = M_V/2f$ the transition potential corresponding to the diagrams of Fig. 1 are given by

$$V_{ab(P_1 B_1 \to P_2 B_2)} = \frac{C_{ab}}{4f^2}(E_{P_1} + E_{P_2}), \tag{2}$$

$$V_{ab(V_1 B_1 \to V_2 B_2)} = \frac{C_{ab}}{4f^2}(E_{V_1} + E_{V_2})\vec{\epsilon}_1 \cdot \vec{\epsilon}_2, \tag{3}$$

where the $a, b$ stand for different channels of $P_1(V_1)B_1$ and $P_2(V_2)B_2$, respectively. The $E$ is the energy of corresponding particle. The $\vec{\epsilon}$ is the polarization vector of the initial or final vector. And the $\epsilon^0_{1,2}$ component is neglected consistently with taking $\vec{p}/M_V \sim 0$, with $\vec{p}$ the momentum of the vector meson. Here we only change the charm quark to beauty quark, so the $C_{ab}$ coefficients are exactly the same as those in Ref.[16], so that there are only two cases, (I, S) = (1/2, 0) and (0, -1), which have attractive potential. We list the values of the $C_{ab}$ coefficients for $PB \to PB$ for these two cases in Table I and Table II, respectively.

TABLE I: Coefficients $C_{ab}$ in Eq. (2) for $(I, S) = (1/2, 0)$

| | $B\Sigma_b$ | $B\Lambda_b$ | $\eta_b N$ | $\pi N$ | $\eta N$ | $\eta' N$ | $K\Sigma$ | $K\Lambda$ |
|---|---|---|---|---|---|---|---|---|
| $B\Sigma_b$ | $-1$ | 0 | $-\sqrt{3/2}$ | $-1/2$ | $-1/\sqrt{2}$ | $1/2$ | 1 | 0 |
| $B\Lambda_b$ | | 1 | $\sqrt{3/2}$ | $-3/2$ | $1/\sqrt{2}$ | $-1/2$ | 0 | 1 |

TABLE II: Coefficients $C_{ab}$ in Eq. (2) for $(I, S) = (0, -1)$

| | $B_s\Lambda_b$ | $B\Xi_b$ | $B\Xi_b'$ | $\eta_b\Lambda$ | $\pi\Sigma$ | $\eta\Lambda$ | $\eta'\Lambda$ | $\bar{K}N$ | $\mathrm{K}\ \Xi$ |
|---|---|---|---|---|---|---|---|---|---|
| $B_s\Lambda_b$ | 0 | $-\sqrt{2}$ | 0 | 1 | 0 | $\sqrt{\frac{1}{3}}$ | $\sqrt{\frac{2}{3}}$ | $-\sqrt{3}$ | 0 |
| $B\Xi_b$ | | $-1$ | 0 | $\sqrt{\frac{1}{2}}$ | $-\frac{3}{2}$ | $\sqrt{\frac{1}{6}}$ | $-\sqrt{\frac{1}{12}}$ | 0 | $\sqrt{\frac{3}{2}}$ |
| $B\Xi_b'$ | | | $-1$ | $-\sqrt{\frac{3}{2}}$ | $\sqrt{\frac{3}{4}}$ | $-\sqrt{\frac{1}{2}}$ | $\frac{1}{2}$ | 0 | $\sqrt{\frac{1}{2}}$ |
| $\eta_b\Lambda$ | | | | 0 | 0 | 0 | 0 | 0 | 0 |

With the transition potential, the coupled-channel scattering matrix can be obtained by solving the coupled-channel Bethe-Salpeter equation in the on-shell factorization approach of Refs.[3, 5]

$$T = [1 - VG]^{-1}V \tag{4}$$

with G being the loop function of a meson (P), or a vector (V), and a baryon (B). The $\vec{\epsilon}_1\cdot\vec{\epsilon}_2$ factor of Eq. (3) factorizes out also in $T$.

For the G loop function, there are usually two ways to regularize it. First one is using dimensional regularization by means of the formula

$$
\begin{aligned}
G &= i2M_B\int\frac{d^4q}{(2\pi)^4}\frac{1}{(P-q)^2-M_B^2+i\varepsilon}\frac{1}{q^2-M_P^2+i\varepsilon},\\
&= \frac{2M_B}{16\pi^2}\Big\{a_\mu+\ln\frac{M_B^2}{\mu^2}+\frac{M_P^2-M_B^2+s}{2s}\ln\frac{M_P^2}{M_B^2}\\
&\quad+\frac{\bar{q}}{\sqrt{s}}\big[\ln(s-(M_B^2-M_P^2)+2\bar{q}\sqrt{s})+\ln(s+(M_B^2-M_P^2)+2\bar{q}\sqrt{s})\\
&\quad-\ln(-s-(M_B^2-M_P^2)+2\bar{q}\sqrt{s})-\ln(-s+(M_B^2-M_P^2)+2\bar{q}\sqrt{s})\big]\Big\}\ ,
\end{aligned}
\tag{5}
$$

where $q$ is the four-momentum of the meson, $P$ the total four-momentum of the meson and the baryon, $s=P^2$, $\bar{q}$ denotes the three momentum of the meson or baryon in the center of mass frame, $\mu$ is a regularization scale, which we put 1000 MeV here. Changes in the scale are reabsorbed in the subtraction constant $a_\mu$ to make results scale independent. $a_\mu$ is of the order of $-2$, which is the natural value of the subtraction constant [18]. When we look for poles in the second Riemann sheet, we should change $q$ to $-q$ when $\sqrt{\mathrm{s}}$ is above the threshold in Eq.(5) [19].

The second way to regularize the $G$ loop function is by putting a cutoff in the three-momentum:

$$
\begin{aligned}
G &= i2M_B\int\frac{d^4q}{(2\pi)^4}\frac{1}{(P-q)^2-M_B^2+i\varepsilon}\frac{1}{q^2-M_P^2+i\varepsilon}\\
&= \int_0^\Lambda\frac{\bar{q}^2d\bar{q}}{4\pi^2}\frac{2M_B(\omega_P+\omega_B)}{\omega_P\,\omega_B\,(s-(\omega_P+\omega_B)^2+i\epsilon)}\ ,
\end{aligned}
\tag{6}
$$

where $\omega_P=\sqrt{\bar{q}^2+M_P^2}$, $\omega_B=\sqrt{\bar{q}^2+M_B^2}$, and $\Lambda$ is the cutoff parameter in the three-momentum of the function loop.

Here we give some detailed discussion on these two types of G function. Firstly the free parameters are $a_\mu$ in Eq.(5) and $\Lambda$ in Eq.(6). The value of $\Lambda$ is around 0.8 GeV, which are within the natural range for effective theories [5]. Then we can choose $a_\mu$ so that the shapes of these two G functions from Eq.(5) and Eq.(6) are almost the same close to threshold and they take the same value at threshold. In Fig.2, the real part and imaginary part of two G functions vs the energy difference between the center mass energy and the corresponding threshold for $K\Sigma$, $\bar{D}\Sigma_c$ and $B\Sigma_b$ channels are demonstrated. In the Table.III, the parameters for different G functions and channels are listed. While the imaginary parts of two G functions are exactly the same, there are some differences for the real parts of two G functions and the differences become bigger for heavier channels. For the same $\Lambda$ value, the magnitude of $a_\mu$ depends on the threshold of channels and gets bigger for heavier channels. One point should be mentioned is that for the $B\Sigma_b$ channel the real part of the G function given by Eq.(5) is larger than zero for energies more than 50 MeV below the threshold as shown in the Fig.2. As we know, if the interaction is repulsive potential, *i.e.*, the value of the potential $V$ is positive, there should be no bound state. However, when the real part of G function is also positive below the threshold, the pole can still be found in the model T matrix with a repulsive potential. These poles far below threshold are beyond the valid region of the model approximation and should be discarded. Since varying the $G$ function in a reasonable range does not influence our conclusion qualitatively, we present our numerical results in the dimensional regularization scheme with $a_\mu = -3.71$, corresponding $\Lambda$ around 0.8 GeV, in this paper.

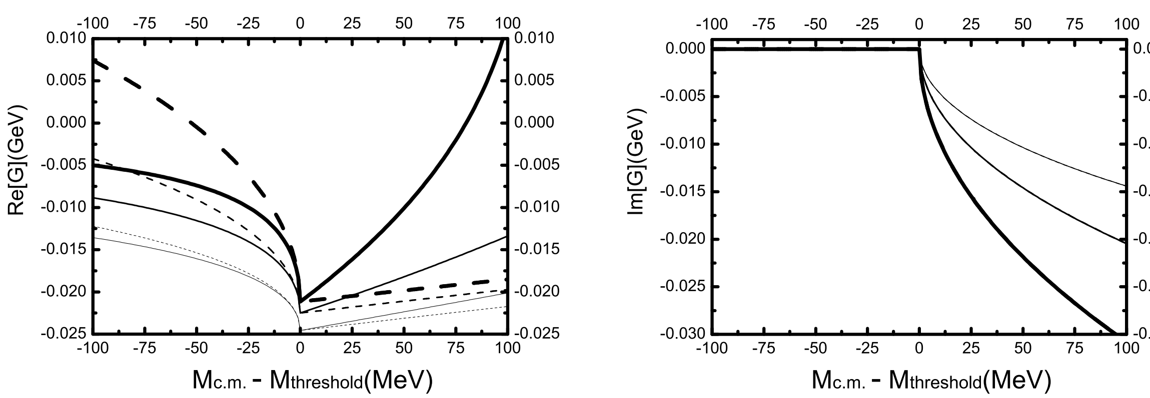


FIG. 2: The real part (left) and imaginary part (right) of two G functions vs the energy difference between the C.M. energy and the threshold energy. The solid lines are for Eq.(6), and dashed lines are for Eq.(5). The thickest lines are for $B\Sigma_b$ channel, the thinnest ones are for $K\Sigma$ channel, and middle ones are for $\bar{D}\Sigma_c$ channel. The used parameters are listed in the Table.III with $\Lambda = 0.8GeV$.

With the potential and $G$ function fixed, the unitary T amplitude can be obtained by Eq.(4). The poles in the $T$ matrix are looked for in the complex plane of $\sqrt{s}$. Those appearing in the first Riemann sheet below threshold are considered as bound states whereas those located in the second Riemann sheet and above the threshold of some channel are identified

TABLE III: The parameters for two types of G functions in the cases of $K\Sigma$, $\bar{D}\Sigma_c$ and $B\Sigma_b$ interactions, with $a_\mu$ for Eq.(5) and $\Lambda$ for Eq.(6). The listed $a_\mu$ and $\Lambda(GeV)$ give the same value of two G functions at the corresponding threshold.

| | Threshold(GeV) | $a_\mu$ | | | | |
|---|---|---|---|---|---|---|
| $\Lambda(GeV)$ | | 0.7 | 0.8 | 0.9 | 1.0 | 1.1 |
| $B\Sigma_b$ | 11.087 | $-3.679$ | $-3.715$ | $-3.751$ | $-3.786$ | $-3.822$ |
| $\bar{D}\Sigma_c$ | 4.231 | $-2.196$ | $-2.283$ | $-2.369$ | $-2.453$ | $-2.536$ |
| $K\Sigma$ | 1.688 | $-1.297$ | $-1.463$ | $-1.619$ | $-1.766$ | $-1.905$ |

as resonances. As previously discussed, the poles will be kept only when the real part of Eq.(5) is negative.

From the T matrix for the $PB \to PB$ and $VB \to VB$ coupled-channel systems, we can find the pole positions $z_R$. Six poles are found in the real axes below threshold and therefore they are bound states. For these cases the coupling constants are obtained from the amplitudes in the real axis. These amplitudes behave close to the pole as:

$$T_{ab} = \frac{g_a g_b}{\sqrt{s} - z_R}. \tag{7}$$

We can use the residue of $T_{aa}$ to determine the value of $g_a$, except for a global phase. Then, the other couplings are derived from

$$g_b = \lim_{\sqrt{s}\to z_R} \left(\frac{g_a T_{ab}}{T_{aa}}\right) . \tag{8}$$

## III. NUMERICAL RESULTS FOR THE SUPER-HEAVY $N^*$ AND $\Lambda^*$

Firstly, we discuss the (I, S) = (1/2, 0) sector. There are 2 channels, $B\Sigma_b$ and $B\Lambda_b$. The masses of these particles are taken from [1], $m_B$ = 5.279 GeV, $m_{B^*}$ = 5.325 GeV, $m_{\Sigma_b}$ = 5.807 GeV and $m_{\Lambda_b}$ = 5.620 GeV. With the approach outlined in the last section, the obtained pole positions $z_R$ and coupling constants $g_\alpha$ are listed in Tables IV for $PB \to PB$ and $VB \to VB$. Because these poles are bound states for each channel, they have zero width when neglecting transitions mediated by t-channel exchange of heavy beauty mesons. To consider some possible decay channels for them, such as $\pi N$, $\eta N$, $K\Sigma$ and so on, we estimate these decays through heavy beauty meson exchanges by means of box diagrams as in Refs.[16, 20, 21]. We neglect transitions to the hidden charm channels such as $\bar{D}\Sigma_c$ and $\bar{D}\Lambda_c^+$, because they need t-channel exchange of too heavy vector meson constituted of charm and beauty quarks. We also do not consider the transitions between $VB$ and $PB$ channels for the same reason as given in Ref.[16]. The results for $PB$ and corresponding $VB$ channels are listed in Table V.

| $z_R$ (MeV) | $g_\alpha$ | |
|---|---|---|
| | $B\Sigma_b$ | $B\Lambda_b$ |
| 11052 | 2.05 | 0 |
| | $B^*\Sigma_b$ | $B^*\Lambda_b$ |
| 11100 | 2.02 | 0 |

TABLE IV: Pole positions $z_R$ and coupling constants $g_a$ for the states in (I, S) = (1/2, 0) sector.

| $M$ (MeV) | $\Gamma$ (MeV) | $\Gamma_i$ (MeV) | | | | |
|---|---|---|---|---|---|---|
| | | $\pi N$ | $\eta N$ | $\eta' N$ | $K\Sigma$ | $\eta_b N$ |
| 11052 | 1.38 | 0.10 | 0.21 | 0.11 | 0.42 | 0.52 |
| | | $\rho N$ | $\omega N$ | $K^*\Sigma$ | $\Upsilon N$ | |
| 11100 | 1.33 | 0.09 | 0.30 | 0.39 | 0.51 | |

TABLE V: Mass ($M$), total width ($\Gamma$), and partial decay widths ($\Gamma_i$) for (I, S) = (1/2, 0) sector.

Then we discuss the (I, S) = (0, -1) sector. There are 3 channels, $B_s\Lambda_b$, $B\Xi_b$ and $B\Xi_b'$. The masses of $B$, $B_s$, $\Xi_b$ and $\Lambda_b$ have been precisely measured and can be taken from Ref.[1]. $m_{B_s} = 5.366$ GeV, $m_{B_s^*} = 5.4128$ GeV and $m_{\Xi_b} = 5.7924$ GeV. The $\Xi_b'$ has not been observed yet. Its mass has been predicted to be 5.922 GeV in Ref.[22] and 5.960 GeV in Ref.[23]. We choose a middle value 5.940 GeV in this paper. From Table II, the $B\Xi_b'$ channel is decoupled from other two channels, so there should be a bound state for this channel, the same as corresponding vector-meson-baryon channel, $B^*\Xi_b'$. For this channel, the results are listed in Table VI.

It is much more complicated to consider T matrix for the coupled $B_s\Lambda_b$ and $B\Xi_b$ channels. The T matrix can be written as:

$$T = \frac{1}{1 - VG_{B\Xi_b}} \begin{pmatrix} V^2_{B_s\Lambda_b \to B\Xi_b} G_{B_s\Lambda_b} & V_{B_s\Lambda_b \to B\Xi_b} \\ V_{B_s\Lambda_b \to B\Xi_b} & V \end{pmatrix} \tag{9}$$

with $V = V_{B\Xi_b \to B\Xi_b} + V^2_{B_s\Lambda_b \to B\Xi_b} G_{B_s\Lambda_b}$.

The $V$ is negative and hence provides an attractive potential. For $a_\mu = -3.71$, one pole is found for the coupled-channel system, with mass between the two thresholds of $B_s\Lambda_b$ (10.986 GeV) and $B\Xi_b$ (11.071 GeV). The pole position depends on the value of $a_\mu$ as demonstrated in Table VI and can move to below the $B_s\Lambda_b$ threshold when the magnitude of $a_\mu$ increases, such as for $a_\mu = -3.82$ corresponding to the $\Lambda = 1.1$ GeV. The coupling constants and the possible decay channels of these two resonances are listed in Tables VII and VIII for $a_\mu = -3.71$. Similarly, the results for the corresponding vector-meson-baryon channels are also listed in Tables VII and VIII for $a_\mu = -3.71$.

| $a_\mu$ | $z_R$ (MeV) | |
|---|---|---|
| | $B_s\Lambda_b$ and $B\Xi_b$ | $B\Xi'_b$ |
| $-3.68$ | $11030 - 0.60i$ | 11198 |
| $-3.71$ | $11021 - 0.59i$ | 11191 |
| $-3.75$ | $11004 - 0.49i$ | 11178 |
| $-3.78$ | $10990 - 0.24i$ | 11167 |
| $-3.82$ | 10970 | 11151 |

TABLE VI: Pole positions $z_R$ with different $a_\mu$ for $PB \to PB$ in (I, S) = (1/2, -1) sector.

Totally two $N^*$ and four $\Lambda^*$ states are predicted to exist with masses above 11 GeV and very narrow widths of only a few MeV. The very narrow widths are due to the fact that all decays are tied to the necessity of the exchange of a heavy beauty vector meson because of hidden $b\bar{b}$ components involved in these states, and hence are suppressed. If these predicted narrow $N^*$ and $\Lambda^*$ resonances with hidden beauty are found, they definitely cannot be accommodated by quark models with three constituent quarks. Together with other possible $N^*$ and $\Lambda^*$ states of other quantum numbers with hidden beauty, they should form

| $z_R$ (MeV) | | $g_\alpha$ | |
|---|---|---|---|
| | $B_s\Lambda_b$ | $B\Xi_b$ | $B\Xi'_b$ |
| $11021-0.59i$ | $0.14-0.11i$ | $2.27+0.004i$ | 0 |
| 11191 | 0 | 0 | 1.92 |
| | $B_s^*\Lambda_b$ | $B^*\Xi_b$ | $B^*\Xi'_b$ |
| $11069-0.59i$ | $0.14-0.12i$ | $2.24+0.005i$ | 0 |
| 11238 | 0 | 0 | 1.89 |

TABLE VII: Pole positions $z_R$ and coupling constants $g_a$ for the states in (I, S) = (1/2, -1) sector for $a_\mu = -3.71$.

| $M$ (MeV) | $\Gamma$ (MeV) | | | $\Gamma_i$ | | (MeV) | | |
|---|---|---|---|---|---|---|---|---|
| | | $\bar{K}N$ | $\pi\Sigma$ | $\eta\Lambda$ | $\eta'\Lambda$ | $K\Xi$ | $\eta_b\Lambda$ | $B_s\Lambda_b$ |
| 11021 | 2.21 | 0.65 | 0.01 | 0.08 | 0.14 | 0.01 | 0.19 | 1.18 |
| 11191 | 1.24 | 0 | 0.28 | 0.18 | 0.10 | 0.18 | 0.48 | 0 |
| | | $\bar{K}^*N$ | $\rho\Sigma$ | $\omega\Lambda$ | $\phi\Lambda$ | $K^*\Xi$ | $\Upsilon\Lambda$ | $B_s^*\Lambda_b$ |
| 11070 | 2.17 | 0.61 | 0.01 | 0.01 | 0.20 | 0.01 | 0.19 | 1.18 |
| 11239 | 1.19 | 0 | 0.26 | 0.26 | 0 | 0.17 | 0.48 | 0 |

TABLE VIII: Mass ($M$), total width ($\Gamma$), and partial decay widths ($\Gamma_i$) for the states in (I, S) = (1/2, -1) sector for $a_\mu = -3.71$.

a super-heavy island of the heaviest masses for excited nucleons $N^*$ and excited hyperons $\Lambda^*$.

## IV. PRODUCTION OF $N^*_{b\bar{b}}$ AND $\Lambda^*_{b\bar{b}}$ IN $pp$ AND $ep$ COLLISIONS

In order to look for these predicted super-heavy $N^*_{b\bar{b}}$ and $\Lambda^*_{b\bar{b}}$ states, we give an estimation of their production cross section in the $pp \to pp\eta_b$ and $ep \to ep\Upsilon$ reactions. The Feynman diagrams are shown in Fig.3. We also estimate the background of the $pp \to pp\eta_b$ with $N^*_{b\bar{b}}$

replaced by the nucleon pole.

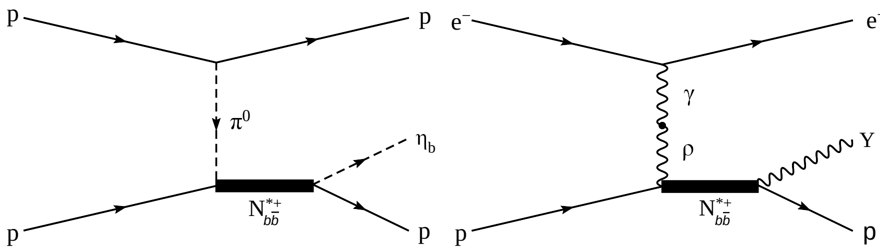


FIG. 3: Feynman diagrams for the reaction $pp \to pp\eta_b$ and $ep \to ep\Upsilon$.

The Lagrangians for the interaction vertices of these two reactions are as follows [24–26]:

$$\begin{aligned}
\mathcal{L}_{NN\pi} &= g_{NN\pi}\bar{N}\gamma_5\vec{\tau}\cdot\vec{\psi}_\pi N + h.c., && (10)\\
\mathcal{L}_{NN\eta_b} &= g_{NN\eta_b}\bar{N}\gamma_5\psi_{\eta_b}N + h.c., && (11)\\
\mathcal{L}_{N^*_{b\bar{b}}N\pi} &= g_{N^{*+}_{b\bar{b}}N\pi}\overline{N^*_{b\bar{b}}}N\vec{\tau}\cdot\vec{\psi}_\pi + h.c., && (12)\\
\mathcal{L}_{N^*_{b\bar{b}}N\eta_b} &= g_{N^{*+}_{b\bar{b}}N\eta_b}\overline{N^*_{b\bar{b}}}N\psi_{\eta_b} + h.c., && (13)\\
\mathcal{L}_{ee\gamma} &= ie\bar{\psi}_e\gamma_5\gamma_\mu\psi_e A^\mu_\gamma + h.c., && (14)\\
\mathcal{L}_{\rho\gamma} &= \frac{em^2_\rho}{f_\rho}\rho^\mu A_{\gamma\mu} + h.c., && (15)\\
\mathcal{L}_{N^*_{b\bar{b}}N\rho} &= g_{N^*_{b\bar{b}}N\rho}\overline{N^*_{b\bar{b}}}\gamma_5\gamma^\mu N\tilde{g}_{\mu\nu}(P_{N^*_{c\bar{c}}})\vec{\tau}\cdot\vec{\psi}^\nu_\rho + h.c., && (16)\\
\mathcal{L}_{N^*_{b\bar{b}}N\Upsilon} &= g_{N^*_{b\bar{b}}N\rho}\overline{N^*_{b\bar{b}}}\gamma_5\gamma^\mu N\tilde{g}_{\mu\nu}(P_{N^*_{c\bar{c}}})\psi^\nu_\Upsilon + h.c.. && (17)
\end{aligned}$$

with $\tilde{g}_{\mu\nu}(P) = -g_{\mu\nu} + \frac{P^\mu P^\nu}{P^2}$.

In our model calculation, we only consider S-wave PB and VB interactions, so the spin-parity $J^P$ of our predicted $N^*_{b\bar{b}}$ for the PB channels is $1/2^-$, and the $N^*_{b\bar{b}}$ for the VB channels can be either $1/2^-$ or $3/2^-$, but assumed to be $1/2^-$ here for a simple estimation of rough production rate. The coupling constants of the Lagrangians can be either calculated from its corresponding partial decay widths or obtained from references. They are all listed in Table IX. For the $NN\eta_b$ vertex, the width of $\eta_b$ has not been measured. Since both $\eta_b$ and $\eta_c$ couple to nucleon through two gluon exchange, we use the relation $g_{NN\eta_b} \sim g_{NN\eta_c}\alpha^4_s(M_{\eta_b})/\alpha^4_s(M_{\eta_c})$ to estimate the $g_{NN\eta_b}$ with $g_{NN\eta_c}$ determined from the decay width of $\eta_c \to p\bar{p}$.

As usual, the off-shell form factors should be considered here. We use two kinds of form

| Vertex | $\Gamma(MeV)$ | Coupling Constant($g^2/4\pi$) |
|---|---|---|
| $pp\pi^0$ | | 14.4 |
| $N^{*+}_{b\bar{b}}p\pi^0$ | 0.033 | $1.03 \times 10^{-5}$ |
| $N^{*+}_{b\bar{b}}p\eta_b$ | 0.52 | $1.81 \times 10^{-3}$ |
| $ee\gamma$ | | 1/137 |
| $\gamma\rho$ | | 2.7 [24] |
| $N^{*+}_{b\bar{b}}p\rho^0$ | 0.030 | $4.42 \times 10^{-4}$ |
| $N^{*+}_{b\bar{b}}p\Upsilon$ | 0.51 | $7.70 \times 10^{-2}$ |
| $pp\eta_b$ | | $1 \times 10^{-6}$ |

TABLE IX: The coupling constants of involved vertices and corresponding widths used.

factors for mesons and baryons, respectively.

$$F_M = \frac{\Lambda_M^2 - m_M^2}{\Lambda_M^2 - p_M^2}, \tag{18}$$

$$F_N = \frac{\Lambda_N^4}{\Lambda_N^4 + (p_N^2 - m_N^2)^2}, \tag{19}$$

where the $M$ stand for $\pi$ or $\rho$, and the $N$ stand for $N^*_{b\bar{b}}$ or nucleon pole. Here $\Lambda_M = 1.3$ GeV, $\Lambda_N = 1.0$ GeV.

To produce the predicted $N^*_{b\bar{b}}(11052)$ in the pp collisions, the center-of-mass energy should be above 12 GeV. In Fig.4, the left figure shows our theoretical estimated total cross section for the $pp \to pp\eta_b$ reaction through the $N^*_{b\bar{b}}$ production vs the center-of-mass energy, with (dashed curve) and without (solid curve) including the off-shell form factors. As an estimation of background contribution to the $N^*_{b\bar{b}}$ production, we also calculate the corresponding cross section through the off-shell nucleon pole without including the form factors. The result is shown by the dotted curve. The contribution from the nuclear pole is much smaller than that from the $N^*_{b\bar{b}}$ production, because the nucleon pole is much more off-shell than $N^*_{b\bar{b}}$. The contribution of the nucleon pole with form factors becomes very small for the same reason, so it is not shown in Fig.4. This background reaction will not influence the observation of the $N^*_{b\bar{b}}$ production, especially for the energy range $13 \sim 25$ GeV. The cross section from $N^*_{b\bar{b}}$ production is about 0.1 nb, which is much smaller than that for the corresponding reaction $pp \to pp\eta_c$ with $N^*_{c\bar{c}}$ production [16] of about 0.1 $\mu b$. The main reason is that both couplings of $N^*_{b\bar{b}}N\pi$ and $N^*_{b\bar{b}}N\eta_b$ are much smaller than the corresponding

$N^*_{c\bar{c}}N\pi$ and $N^*_{c\bar{c}}N\eta_c$ couplings. These two vertices cause a reduction of about 2 orders of magnitude. In addition, because the center-of-mass energy here is much larger than that in the previous calculation for the $\eta_c$ production, the propagator of exchanged $\pi^0$ further reduce the contribution. For the same reason, the contribution with form factors is much less than that without them.

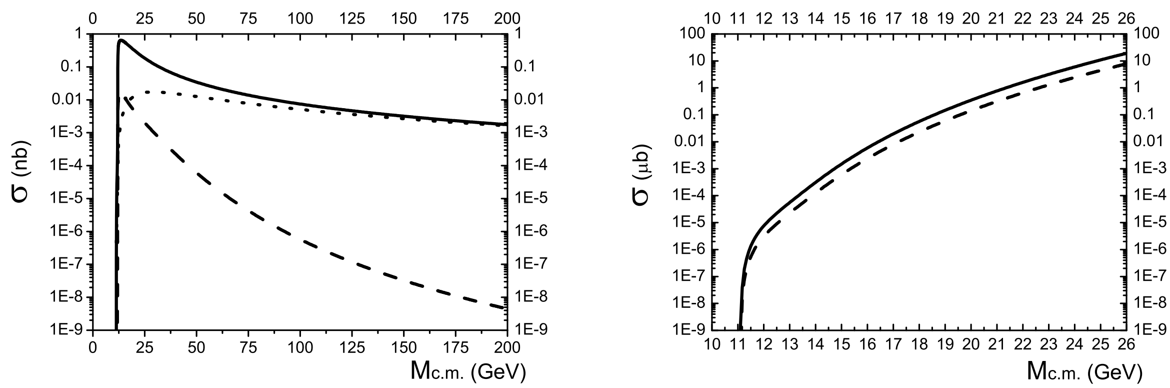


FIG. 4: Total cross section vs invariant mass of system for $pp \to pp\eta_b$ reaction (left) and $e^-p \to e^-p\Upsilon$ reaction (right), with (dashed curves) and without (solid curves) including off-shell form factors, through production of the predicted $N^*_{b\bar{b}}$ resonances. The dotted curve is the background contribution from the nucleon pole for the $pp \to pp\eta_b$ reaction without including form factors.

For the production of $N^*_{b\bar{b}}(11100)$ in $ep$ collisions, the invariant mass of the system should be above 11 GeV. The right figure in Fig.4 shows our calculated total cross section for the $e^-p \to e^-p\Upsilon$ reaction vs the invariant mass of the system with (dashed curve) and without (solid curves) including form factors. The cross section of this reaction is much larger than that for the $pp \to pp\eta_b$ reaction. The reason is due to the propagator of massless photon. The propagator of photon is given as the following:

$$\frac{1}{p_\gamma^2} = \frac{1}{2(m_e^2 + p_i p_f cos\theta - E_i E_f)}, \tag{20}$$

where the $p_i$, $E_i$ are the three-momentum and energy of initial $e^-$, and $p_f$, $E_f$ for final $e^-$. $\theta$ is the angle between initial and final $e^-$. When the directions of initial and final $e^-$ are the same, *i.e.*, $cos\theta = 1$, the value of Eq.(20) becomes very large because of the very small mass of $e^-$. As the beam momentum of $e^-$ becomes larger, the propagator of photon can reach very big value. For the invariant mass of the system less than 15 GeV, the cross section of $e^-p \to e^-p\Upsilon$ reaction is of the same order of magnitude as that of $pp \to pp\eta_b$ reaction.

## V. SUMMARY

In summary, the meson-baryon coupled channel unitary approach with the local hidden gauge formalism is extended to the hidden beauty sector. Two $N^*_{b\bar{b}}$ states and four $\Lambda^*_{b\bar{b}}$ states are predicted to be dynamically generated from coupled PB and VB channels with the same approach as for the hidden charm sector [16]. Because of the hidden $b\bar{b}$ components involved in these states, the masses of these states are all above 11 GeV while their widths are of only a few MeV, which should be form the heaviest island for the quite stable $N^*$ and $\Lambda^*$ baryons. The nature of these states is similar as corresponding $N^*_{c\bar{c}}$ and $\Lambda^*_{c\bar{c}}$ states predicted in Ref.[16], which definitely cannot be accommodated by the conventional 3q quark models.

Production cross sections of the predicted $N^*_{b\bar{b}}$ resonances in $pp$ and $ep$ collisions are estimated as a guide for the possible experimental search at relevant facilities in the future. For the $pp \to pp\eta_b$ reaction, the best center-of-mass energy for observing the predicted $N^*_{b\bar{b}}$ is 13 $\sim$ 25 GeV, where the production cross section is about 0.01 nb. For the $e^-p \to e^-p\Upsilon$ reaction, when the center-of-mass energy is larger than 14 GeV, the production cross section should be larger than 0.1 nb. Nowadays, the luminosity for pp or ep collisions can reach $10^{33}cm^{-2}s^{-1}$, this will produce more than 1000 events per day for the $N^*_{b\bar{b}}$ production. We expect future facilities, such as proposed electron-ion collider (EIC) [27], to discover these very interesting super-heavy $N^*$ and $\Lambda^*$ with hidden beauty.

**Acknowledgments**

This work is supported by the National Natural Science Foundation of China (NSFC) under grants Nos. 10875133, 10821063, 11035006 and by the Chinese Academy of Sciences under project No. KJCX2-EW-N01, and by the Ministry of Science and Technology of China (2009CB825200).

---

[1] Particle Data Group, K. Nakamura *et al.*, J. Phys. G **37**, 075021 (2010).

[2] N. Kaiser, P. B. Siegel and W. Weise, Phys. Lett. B **362**, 23 (1995).

[3] E. Oset and A. Ramos, Nucl. Phys. A **635**, 99 (1998).

[4] J. A. Oller, E. Oset and A. Ramos, Prog. Part. Nucl. Phys. **45**, 157 (2000).

[5] J. A. Oller and U. G. Meissner, Phys. Lett. B **500**, 263 (2001).

[6] T. Inoue, E. Oset and M. J. Vicente Vacas, Phys. Rev. C **65**, 035204 (2002)

[7] C. Garcia-Recio, M. F. M. Lutz and J. Nieves, Phys. Lett. B **582**, 49 (2004).

[8] T. Hyodo, S. I. Nam, D. Jido and A. Hosaka, Phys. Rev. C **68**, 018201 (2003)

[9] C. Helminen and D. O. Riska, Nucl. Phys. A **699**, 624 (2002).

[10] B. C. Liu, B. S. Zou, Phys. Rev. Lett. **96**, 042002 (2006); ibid, **98**, 039102 (2007).

[11] B. S. Zou, Nucl. Phys. A **835**, 199 (2010).

[12] N. Kaiser, P. B. Siegel and W. Weise, Phys. Lett. B **362**, 23 (1995) [arXiv:nucl-th/9507036].

[13] T. Inoue, E. Oset and M. J. Vicente Vacas, Phys. Rev. C **65**, 035204 (2002) [arXiv:hep-ph/0110333].

[14] J. Nieves and E. Ruiz Arriola, Phys. Rev. D **64**, 116008 (2001)

[15] L. S. Geng, E. Oset, B. S. Zou and M. Doring, Phys. Rev. C **79**, 025203 (2009) [arXiv:0807.2913 [hep-ph]].

[16] J. J. Wu, R. Molina, E. Oset and B. S. Zou, Phys. Rev. Lett. **105**, 23**** (2010), arXiv:1007.0573 [nucl-th]; arXiv:1011.2399 [nucl-th].

[17] E. Oset and A. Ramos, Euro. Phys. J. A **44**, 445 (2010).

[18] J. A. Oller and U. G. Meissner, Phys. Lett. B **500**, 263 (2001) .

[19] L. Roca, E. Oset and J. Singh, Phys. Rev. D **72**, 014002 (2005)

[20] R. Molina, D. Nicmorus and E. Oset, Phys. Rev. D **78**, 114018 (2008)

[21] L. S. Geng and E. Oset, Phys. Rev. D **79**, 074009 (2009)

[22] Z. G. Wang, Phys. Lett. B **685**, 59 (2010) [arXiv:0912.1648 [hep-ph]].

[23] E. E. Jenkins, Phys. Rev. D **54**, 4515 (1996) [arXiv:hep-ph/9603449].

[24] J. J. Xie, C. Wilkin and B. S. Zou, Phys. Rev. C **77**, 058202 (2008) [arXiv:0802.2802 [nucl-th]].

[25] B. S. Zou and F. Hussain, Phys. Rev. C **67**, 015204 (2003) [arXiv:hep-ph/0210164].

[26] J. J. Wu, Z. Ouyang and B. S. Zou, Phys. Rev. C **80**, 045211 (2009).

[27] V. Ptitsyn, AIP Conf. Proc. **1149**, 735 (2009).